A Photonic-Doping-Inspired SIW Antenna With Length-Invariant Operating Frequency

Ziheng Zhou and Yue Li, *Senior Member, IEEE*

***Abstract*— This article presents a novel substrate-integrated waveguide (SIW) antenna with a designable broadside pattern at a length-irrelevant operating frequency, which is inspired from the concept of photonic doping, i.e., embedding a dielectric impurity into the epsilon-near-zero (ENZ) medium. In our design, a section of SIW operating around its cutoff frequency imitates the ENZ host, while a high-permittivity dielectric block is "doped" into the SIW to control the overall field distributions, achieving a sharp 180° phase shift of electric field at the predesigned half- wavelength resonance. Owing to the infinite wavelength in the ENZ medium, the operating frequency of the proposed antenna is irrelevant to its length. In this way, the broadside radiation of the proposed antenna allows to be configured at the same frequency via simply altering the length of the SIW, i.e., the spacing between two radiating apertures. Systematic studies show that the directivity of the proposed antenna can be manipulated over a range from around 6 dBi to almost 10 dBi, along with the half-power beamwidth reduced from 110° to 20°, for the length of the antenna varying from $0.2\lambda_0$ (λ_0 is the wavelength in free space at 5.5 GHz) to $1.2\lambda_0$.**

***Index Terms*— Epsilon-near-zero (ENZ) medium, flexible antennas, photonic doping, radiation pattern, zero-order resonance.**

I. Introduction

THE development of the metamaterial [1], [2] in the past decades has opened up new horizons for the manipulation of electromagnetic wave in an unprecedented way, and one exciting field among which is the rise of metamaterial-based antennas with unusual functionalities. The single-negative and double-negative metamaterials [3], [4] with one or both of permittivity and permeability being negative, have been introduced for the design of miniaturized antennas [5]–[7] and backfire-to-endfire scanning arrays [8]. The 2-D metamaterials, i.e., metasurfaces [9], are employed to empower antennas with stealth property [10], [11] and other performance such as low mutual coupling [12] and dynamic tunability [13]. As an emerging hotspot in the metamaterial family, the epsilon-near-zero (ENZ) material [14]–[18] is drawing increasing interests of physicists and engineers, due to the exotic wave phenomenon yielded from its extreme low constitutive parameter. As the permittivity of the material approaches to 0, the wavelength as well as phase velocity of electromagnetic wave turn to be infinitely large, resulting in a temporally oscillating while spatially static wave dynamics, i.e., effective decoupling of time and space. In addition to those exotic phenomena, ENZ medium has offered exciting opportunities for the advanced applications such as gain enhancement [19]–[22], improving impedance matching for antennas [23]–[25], and shaping radiation patterns at will [26], [27], and flexible devices [28]. Beam steering with ENZ lens [29] and wideband tuning of ENZ tunneling frequency [30], [31] were also actively investigated.

Recently, the methodology named photonic doping [32] is proposed for controlling the field configuration over ENZ region. In this scheme, via an arbitrarily placed macroscopic dielectric "dopant" in the ENZ "host," the total magnetic flux of the system can be altered locally, effectively leading to either the epsilon-and-mu-near-zero (EMNZ) behavior characterized by a geometry-invariant supercoupling effect or the perfect-magnetic-conductor (PMC) behavior that absolutely blocks the power transmission. In the latest research [33], photonic doping was applied for the wave manipulation in a guided wave scenario, where a planar flexible transmission line and a sensitive dielectric sensor were developed.

In this article, we introduce the concept of photonic doping into the invention of a broadside-pattern antenna, named doped ENZ antenna, which features an operating frequency interestingly decoupled from the spacing of radiating apertures. Concretely, we harness a substrate-integrated waveguide (SIW) [34] with two ends open to emulate the ENZ condition around its cutoff frequency [35], which manifests an invariant field along the SIW. Then, the dielectric dopant, a half-wavelength ceramic resonator, is embedded into the SIW to inverse the phase of electric field sharply. In this manner, the effective magnetic currents on the radiating aperture are exactly in phase, yielding a broadside radiation pattern. Different from traditional two-element magnetic current antenna, such as patch antenna [36], the gain and beamwidth of doped ENZ antenna allows to be manipulated flexibly, owing to the peculiar geometry-invariant ENZ property. As a proof of concept, doped ENZ antennas operating near the same frequency $f_0 = 5.5$ GHz with various length L of $0.22\lambda_0$, $0.50\lambda_0$,

Manuscript received December 23, 2019; accepted February 18, 2020. Date of publication March 9, 2020; date of current version July 7, 2020. This work was supported in part by the National Natural Science Foundation of China under Grant 61771280, in part by the Natural Science Foundation of Beijing Manipulate under Contract 4182029, and in part by the Tsinghua University Initiative Scientific Research Program under Contract 2019Z08QCX16. *(Corresponding author: Yue Li.)*

The authors are with the Department of Electronic Engineering, Tsinghua University, Beijing 100084, China, and also with the Beijing National Research Center for Information Science and Technology, Tsinghua University, Beijing 10084, China (e-mail: lyee@tsinghua.edu.cn).

Color versions of one or more of the figures in this article are available online at http://ieeexplore.ieee.org.

Digital Object Identifier 10.1109/TAP.2020.2977746

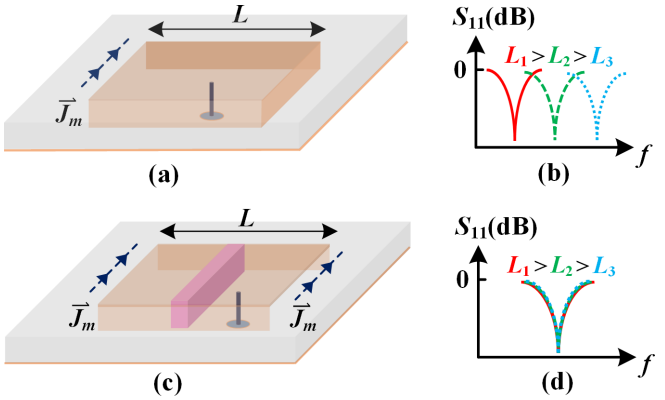

Fig. 1. (a) Schematic of a planar waveguide antenna with one open end and (b) reflection coefficients under different lengths L. (c) Proposed doped ENZ antenna embedded with a dielectric block and (d) reflection coefficients under different lengths L.

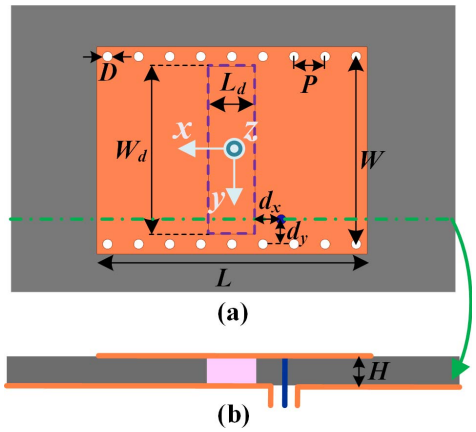

Fig. 2. (a) Top view and (b) cross-sectional view of the designed doped ENZ antenna.

and $0.72\lambda_0$ (λ_0 is the wavelength in free space at f_0) are fabricated and tested. The measurement results show that, with the length increased, realized gain of the prototyped antenna rises from 5.8 dBi ($L = 0.22\lambda_0$) to almost 10 dBi (9.6 dBi for $L = 0.50\lambda_0$ and 8.9 dBi for $L = 0.72\lambda_0$), while the half-power beamwidth (HPBW) of the main lobe is reduced notably from 110° to 20°, which are in agreement with the simulation and analytical model. Additionally, the measured peak efficiencies of the antennas are higher than 80%. With devisable radiation properties at a fixed frequency, the proposed doped ENZ antenna can exhibit potentials for various applications such as intelligent wireless communication and sensing.

The rest of this article is organized as follows. Section II introduces the concept of the doped ENZ antenna and sheds light on its operating mechanism via analytical modeling and full-wave simulation. In Section III, we experimentally verified the designable radiation properties of the proposed antenna at a fixed frequency via changing its length. Finally, Section IV summarizes this article.

II. Theory and Antenna Design

A. Concept of Doped ENZ Antenna

To better introduce the motivation of this article, we start with fundamental microstrip antennas [36]–[42], which are planar magnetic current arrays with specific distributions. As a knowledge well known in the textbook, the traditional rectangular patch antenna [36], [37], a typical kind of microstrip antenna, operates at the fundamental TM^z_{100} mode under the condition that the length of the patch is about half wavelength in the substrate. For this reason, the electrical length of the distance between two radiating apertures is strictly fixed, leading to roughly determined radiation properties in terms of directivity and beamwidth. Another case familiar to us is the planar waveguide antenna with one open aperture, whose structure is presented in Fig. 1(a). At the resonance, the electric field reaches its maximum value on the open aperture while vanishing on the shorting wall at the other end of the waveguide. In this scenario, the resonant frequency becomes lower as the antenna length increases, as illustrated in Fig. 1(b).

A fundamental question is naturally raised that: is it possible to decouple the arrangement of radiating apertures with the operating frequency for more degrees of freedom to tailor the antenna's radiation behavior? To address this problem, we propose the concept of the doped ENZ antenna, whose 3-D perspective view is exhibited in Fig. 1(c). First, we design the radiating apertures with changeable spacing at the same frequency via the architecture of a waveguide at its cutoff frequency. Since the electric field within the pure waveguide-emulated ENZ medium is always unchanged along the SIW, we would get a pair of antiparallel magnetic currents at the radiating apertures, which leads to a differential radiation pattern with a null at the broadside [26]. To address this problem, in the second step, we introduce a macroscopic dielectric "dopant," a half-wavelength resonator, into the ENZ "host," for tuning the field distribution and realizing in-phase radiation at two apertures. In this manner, the proposed doped ENZ antenna based on doped ENZ medium would share a similar broadside radiation pattern with popular microstrip antennas while taking an advantage of a length-irrelevant operating frequency, as schematically illustrated in Fig. 1(d).

B. Antenna Geometry and Operating Mechanism

The practical structure of the doped ENZ antenna employs the SIW, and proposed configuration is shown in Fig. 2, where Fig. 2(a) and (b) illustrates, respectively, the top of the antenna and a cross-sectional cut plane containing the feeding pin. The ceramic block with a volume of $L_d \times W_d \times H = 4.8$ mm $\times$ 17.5 mm $\times$ 3 mm is inserted into the substrate with a dielectric constant ε_r of 2.2 and a loss tangent of 0.002. The metallic vias with a diameter $D = 1.0$ mm are arranged with a periodicity $P = 3.0$ mm to serve as the metallic wall, while the spacing W of two rows of vias is 18.8 mm. The feeding probe is positioned with an offset distance $d_x = 2.6$ mm from the ceramic block and $d_y = 3.0$ mm from the metallic vias. The size of the ground is set as 110 mm $\times$ 70 mm. As the geometry of the SIW is given, the dispersive permittivity of the waveguide-emulated plasmonic material is expressed as follows [35]:

$$\varepsilon_{eff}(f) = \varepsilon_r\left(1 - f_0^2/f^2\right). \quad (1)$$

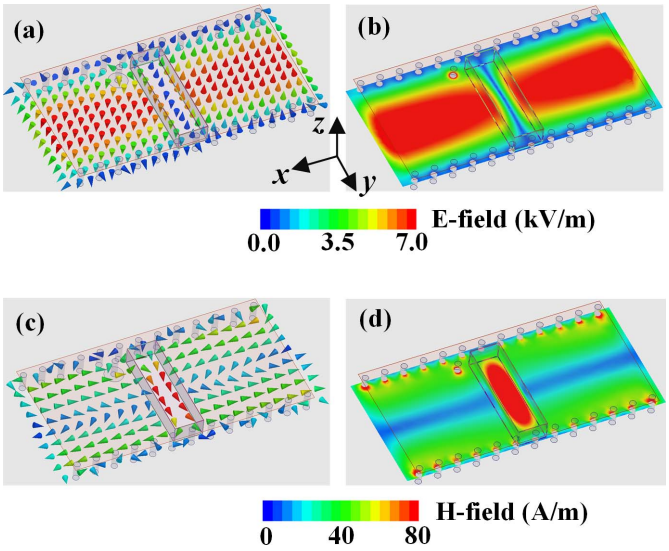

Fig. 3. (a) Simulated electric field vector distribution and (b) magnitude distribution over the structure of the doped ENZ antenna at $f_0 = 5.5$ GHz. (c) Simulated magnetic field vector distribution and (d) magnitude distribution over the structure at $f_0 = 5.5$ GHz.

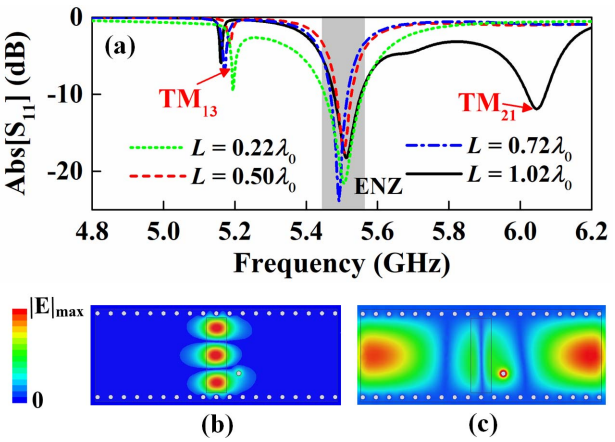

Fig. 4. (a) Simulated reflection coefficients of the doped ENZ antenna with various lengths L. The electric field magnitude distribution at TM_{13} mode of the dielectric block and TM_{21} mode of the SIW are shown in (b) and (c), respectively.

Here, f_0 is the cutoff frequency of the SIW (also the zero of the permittivity function), calculated by

$$f_0 = c/\left(2\sqrt{\varepsilon_r} W_{eff}\right) \tag{2}$$

where c is the speed of light in vacuum, ε_r is the relative permittivity of the substrate, and W_{eff} is the effective width of the SIW given by [34]

$$W_{eff} = W - D^2/(0.95 \cdot P) \tag{3}$$

where W, D, and P are aforementioned geometry parameters marked in Fig. 2(a). Substituting the values of those parameters into (2) and (3), the cutoff frequency f_0 of the waveguide, namely, the frequency where the SIW offer ENZ environment, is calculated to be 5.5 GHz according to (2). It is noted that, under the ENZ condition, the electric field within the cavity is invariant along the length of the waveguide. To enable in-phase radiating magnetic currents on the two open apertures with opposite normal vectors, the inserted dielectric dopant (the ceramic block) should resonate at its TM^z_{110} mode, where the phase of electric field is inversed within the dopant. We have to ensure that the ENZ frequency coincides with the resonance frequency of the dopant

$$f\left(TM^z_{110}\right) = \frac{c}{2\sqrt{\varepsilon_d}}\sqrt{\frac{1}{W_d^2} + \frac{1}{L_d^2}}. \tag{4}$$

The dimensions as well as the relative permittivity ($\varepsilon_d = 34$) of the dopant have been carefully selected, so as to better comply with the constrain $f_0 = f(TM^z_{110})$.

Up to this point, we have expounded the principle for judiciously selecting parameters of the antenna structure, and next, it is beneficial to examine the field configuration for the ENZ resonance at f_0. The full-wave simulation is carried on the commercial software HFSS 15. The proposed antenna structure is placed in an air box with a size of $3.7\lambda_0 \times 3.7\lambda_0 \times \lambda_0$, and radiation boundary is imposed on the surfaces of the air box. The maximum number of tetrahedral mesh elements is 60 000, and the stopping criterion is for the maximum variation of scattering parameters smaller than 0.02. As exhibited in Fig. 3(a) and (b), the electric field maintains constant along the SIW (the region outside of the dopant), resulted from the cutoff waveguide: the traveling and evanescent wave are, respectively, allowed above and below the cutoff frequency while the spatial-static mode along the SIW is supported at the cutoff frequency. We also observed a typical half-wavelength distributed resonant mode within the ceramic block along its x- and y-dimensions, where electric field is inversed by 180° and presents a null at the central plane of the block. That implies, via doping a macroscopic impurity locally, we are able to impact overall field configuration outside, and, meanwhile, retain the ENZ property of the cutoff waveguide (the ENZ host). The field distribution of this cutoff TE_{10} mode also implies that the feeding resistance is too high on the middle plane of the SIW and too low when the probe is close to metallic walls. By tuning the distance (d_y) of the feeding probe to the side metallic wall, a suitable position is determined where the feeding resistance is equal to 50 Ω. The magnetic field vector distribution and magnitude distribution are reported in Fig. 3(c) and (d), respectively, from which we discover that magnetic field is strongly enhanced within this nonmagnetic dielectric dopant on its TM^z_{110} mode, due to the sharp contrast in the permittivity of the ENZ host and the dopant.

Owing to infinite wavelength in the ENZ medium, the operating frequency of the proposed antenna is insensitive to the change of the length of SIW, which can alternatively be interpreted as the effect of zeroth-order resonance. As shown in Fig. 4(a), the doped ENZ antenna stably retains its impedance-matching band for ENZ resonance (highlighted by the gray zone) around the predesigned frequency f_0, even though the length L has varied over an appreciable range from $0.22\lambda_0$ to $1.02\lambda_0$. The nonradiating TM^z_{130} mode is observed in the reflection spectrum, and its electric field distribution is reported in Fig. 4(b). It is noteworthy that the length-invariant working frequency is a unique property of the ENZ resonance,

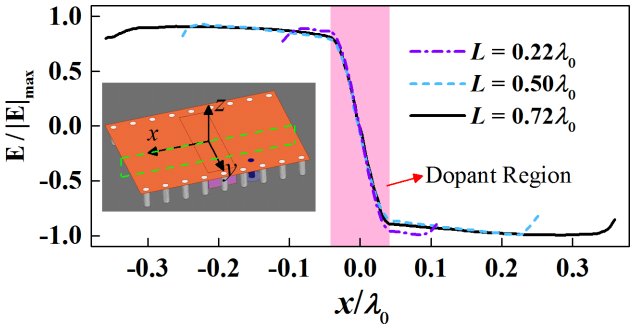

Fig. 5. Simulated values of electric field varying along the x-axis within the middle cut plane (green dashed frame in the inset) of the doped ENZ antenna with different lengths.

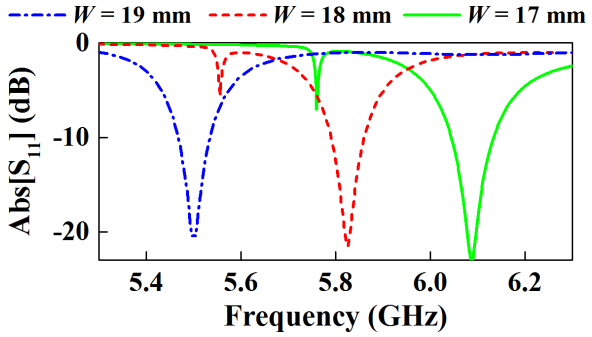

Fig. 6. Simulated reflection coefficients of the doped ENZ antenna with different widths W of the SIW. The corresponding sizes of the dielectric dopant (W_d, L_d) for the cases of $W = 19$ mm, 18 mm, and 17 mm are (17.5, 4.8) mm, (16.5, 4.6) mm, and (15.0, 4.4) mm, respectively.

while the frequencies of higher order modes, such as TM_{21} mode whose electric field configuration is shown in Fig. 4(c), do become notably lower as the spacing of two radiating apertures increases. The simulated values of electric field on the middle cut plane of the antennas with different lengths are reported in Fig. 5. As seen, even though the length of the antenna is stretched by two times, the electric field only changes its phase within the dopant region while maintaining almost a constant value over the undoped ENZ region. The minor variation of the electric field value at the edge of the patch is due to the imperfect open boundary on the aperture. That actually indicates an interesting functionality of spatially static ENZ medium to "extract" or "copy" the field distribution from the surface of a dielectric resonator to another aperture away from that resonator body.

To shed more light into the operating mechanism, we also clarify here that the operating frequency of ENZ resonance is related to the width of the SIW, which determines the cutoff frequency of the SIW. The parametric study is performed to investigate the simulated reflection coefficients of the proposed antenna under different widths. It is necessary to bear in mind that, for keeping the half-wavelength resonance frequency of the dopant the same as cutoff frequency of the SIW, the size of dopant should be altered accordingly. The sizes of the dielectric dopant (W_d, L_d) for SIW with different widths of $W = 19$ mm, 18 mm, and 17 mm are chosen as (17.5, 4.8) mm, (16.5, 4.6) mm, and (15.0, 4.4) mm, respectively. As shown in Fig. 6, for the antenna with smaller width W, its central operating frequency shifts to higher frequency region.

C. Designable Radiation Properties at the Fixed Frequency

Let us recall the electric field configuration demonstrated in Fig. 3(a), where the electric field is antiphase at the two apertures with the antiparallel normal vectors. As a result, the effective radiating magnetic currents are constructively superimposed, contributing to a broadside radiation pattern. Essentially different from the traditional microstrip antenna, the operating frequency of the doped ENZ antenna is irrelevant to the distance of two radiating apertures, owing to the zeroth-order resonance. Fig. 7(a)–(c) presents the simulated 3-D realized gain patterns of the doped ENZ antenna with different lengths L at the same predesigned frequency $f_0 = 5.5$ GHz. The radiation pattern of the antenna with a very small $L(= 0.22\lambda_0, \lambda_0$ is the wavelength in free space at $f_0)$ exhibits a quite broad beamwidth in the upper space, benefiting the application of wide-angle coverage. As the length increases to $0.5\lambda_0$, the realized gain of the antenna rises to 10 dBi, potentially intended for the gain enhancement deployment or point-to-point wireless communication. With size along the SIW being enlarged further, e.g., to $0.72\lambda_0$, the main beam orientated at broadside direction turns to be much narrower, meanwhile accompanied by the emerging side lobes. As seen, the proposed antenna is able to adapt different application scenarios via simply changing its length.

To offer a quantitative explanation of the property of this flexibly designable radiation pattern, we establish a theoretical model of the proposed doped ENZ antenna.

According to the mode analysis in Section II-B, the electric field configuration over the doped ENZ cavity shown in Fig. 3(a) can be formulated as follows:

$$\vec{E} = \begin{cases} \hat{z}E_0\cos(\pi y/W_{eff}); & -L/2 < x < -L_d/2 \\ \hat{z}E_0\cos(\pi y/W_{eff})\sin(\pi x/L_d); & -L_d/2 < x < L_d/2 \\ -\hat{z}E_0\cos(\pi y/W_{eff}); & L_d/2 < x < L/2 \end{cases} \tag{5}$$

and the effective magnetic currents density at the either one of the radiating aperture is calculated according to

$$\vec{M} = -2\hat{n} \times \vec{E}\,|_{x=\pm L/2} = \hat{y}2E_0\cos(\pi y/W_{eff}) \tag{6}$$

where we have taken into account the effect of the metallic ground by multiplying a factor of 2. By integrating the product of current distribution and the Green function of Helmholtz equation [36] over the source region, we then obtain the vector potential and the radiated electric field:

$$\vec{A_m} = \frac{H}{4\pi}\int_{-W_{eff}/2}^{W_{eff}/2} \vec{M}\frac{e^{-jk_0[\sin(\theta)\sin(\varphi)y+r]}}{r}\mathrm{d}y$$
$$\vec{E} = -\nabla \times \vec{A_m} \tag{7}$$

where r is the distance relating the source point and the observation point at the far field; θ and φ denote, respectively, the elevation angle and the azimuth angle [with respect to the coordinate system illustrated in Fig. 7(a)]. We have used the condition in (7) that the height of the aperture is much smaller

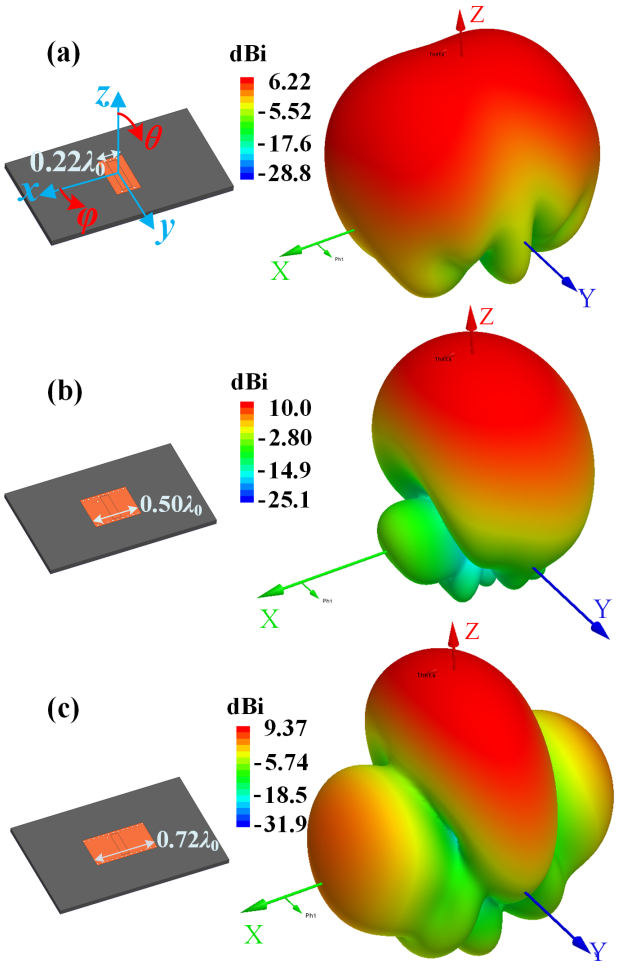

Fig. 7. Simulated 3-D realized gain patterns of the doped ENZ antennas with different lengths (a) $L = 0.22\lambda_0$, (b) $0.50\lambda_0$, and (c) $0.72\lambda_0$ at $f_0 = 5.5$ GHz. λ_0 is the wavelength in free space at f_0.

than the wavelength. Then, the far-field radiation pattern of one aperture is derived as

$$F_e(\theta,\varphi) = \frac{\cos[\pi W_{eff}\sin(\theta)\sin(\varphi)/\lambda_0]}{1-[2W_{eff}\sin(\theta)\sin(\varphi)/\lambda_0]^2} \times \sqrt{1-(\sin(\theta)\sin(\varphi))^2}. \quad (8)$$

It is noteworthy that, since the proposed doped ENZ antenna is a two-element magnetic current array, the total radiation pattern should include the array factor

$$F_a(\theta,\varphi) = \cos[\pi(l+2\Delta l)\sin(\theta)\cos(\varphi)/\lambda_0] \quad (9)$$

where Δl depicts extended length in the substrate evaluated by an empirical formula [37]

$$\Delta l \approx 0.412H\cdot\left(\frac{\varepsilon_e+0.3}{\varepsilon_e-0.258}\right)\left(\frac{W/H+0.264}{W/H+0.8}\right) \quad (10)$$

where ε_e is the effective permittivity approximately given as [37]

$$\varepsilon_e = \frac{\varepsilon_r+1}{2}+\frac{\varepsilon_r-1}{2}\left(1+12\frac{H}{W}\right)^{-1/2}. \quad (11)$$

The radiation pattern of the proposed antenna can finally be yielded from the product of the element factor [(8)] and the array factor [(9)], and then the directivity is calculated by [36]

$$D = \frac{4\pi}{\int_0^{2\pi}\int_0^{\pi/2}[F_e(\theta,\varphi)\cdot F_a(\theta,\varphi)]^2\sin(\theta)d\theta d\varphi}. \quad (12)$$

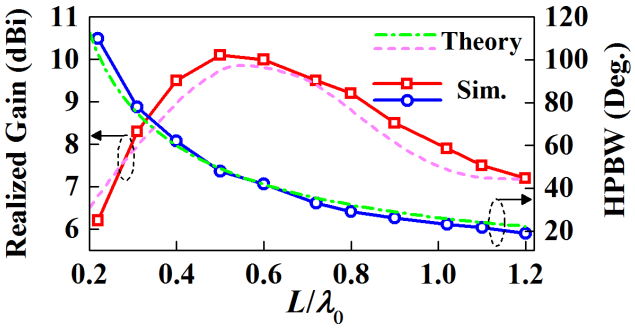

Fig. 8. Simulated and calculated results for the realized gain and HPBW of doped ENZ antenna with different lengths at $f_0 = 5.5$ GHz.

The calculated and the directivity and the HPBW together with the numerically simulated counterparts of the doped ENZ antenna are gathered in Fig. 8. The calculated (simulated) result indicates that directivity of the antenna rises from 6.5 dBi (6.2 dBi) up to 9.7 dBi (10 dBi) as the length L increases from $0.2\lambda_0$ to $0.53\lambda_0$ ($0.50\lambda_0$); meanwhile, the HPBW reduces from near 110° to 20° or so, for the length of antenna varying from $0.22\lambda_0$ to $1.20\lambda_0$. The minor discrepancy between the simulation and calculation can be caused by the impact from the finite-size ground and the minor inaccuracy when treating the edge effect of electric field at the radiating apertures. Even so they are largely in agreement with each other. It is admitted that the nonuniform distribution of electric field on radiating apertures at the cutoff TE_{10} mode would not yield an optimal aperture efficiency. Nevertheless, by flexibly altering the aperture spacing, we optimize the array factor and attain a high directivity of near 10 dBi, on the basis of a simple antenna element. In short, it is concluded that an appreciable range for manipulating the gain and beamwidth of a two-element magnetic current array at the fixed frequency can be achieved via our design.

D. Position-Invariant Doping

To end this section, we discuss briefly another interesting property of the proposed antenna yielded from the photonic doping: position-invariant for the macroscopic dopant. The asymptotically infinite wavelength in the ENZ medium can effectively shrink the space equivalent to a point [16] when analyzing the wave dynamics. So, it is intuitive to expect that any position in the effective ENZ cavity is identical for the photonic dopant. As shown in the inset of Fig. 9(a), we move the dopant away from the center of the SIW along the x-axis with different distances d. The simulated operating frequency of the antenna, shown in Fig. 9(a), well maintains around the predesigned frequency f_0 for distance d varying from 0 to 20 mm ($0.37\lambda_0$). The realized gain patterns of the antenna under different values of d are also investigated, with the simulated patterns on xz and yz planes being presented in Fig. 9(b) and (c), respectively. As seen, the location of the dopant does not influence the radiation property of the doped ENZ antenna.

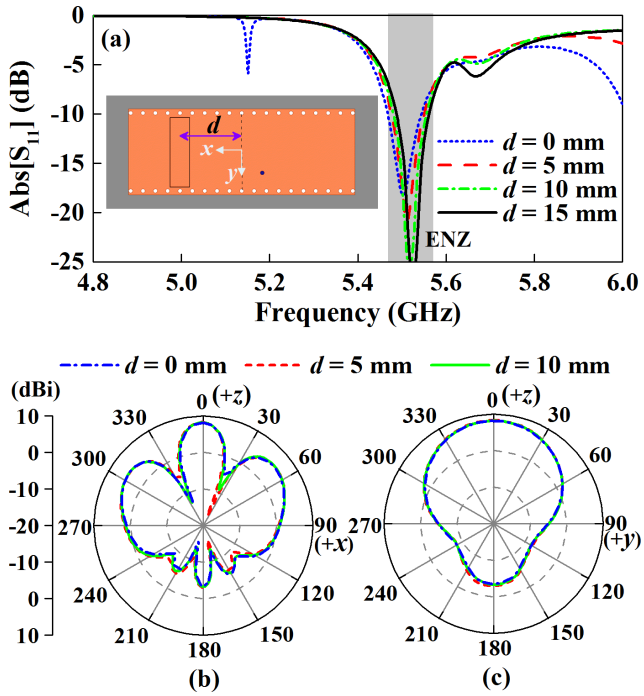

Fig. 9. (a) Simulated reflection coefficients of the doped ENZ antenna ($L = 1.02\lambda_0$) for the dielectric dopant placed at different distances d from the center of the patch. Simulated realized gain patterns on (b) xz plane and (c) yz plane of the antenna for $d = 0$ mm, $d = 5$ mm, and $d = 10$ mm.

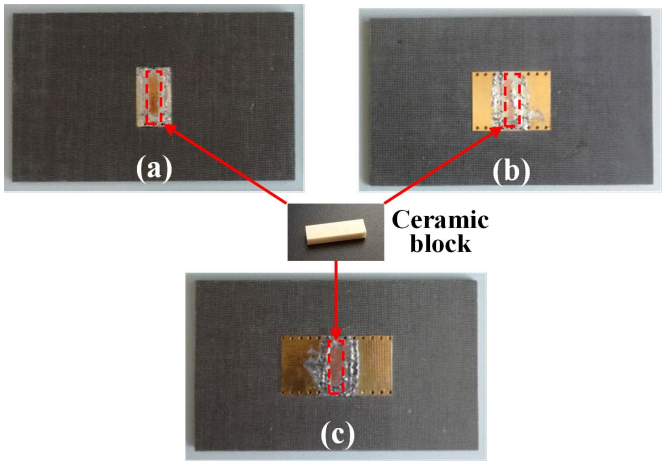

Fig. 10. Photographs of the fabricated prototypes of the doped ENZ antennas with different lengths $L = 0.22\lambda_0$ (a), $0.50\lambda_0$ (b), and $0.72\lambda_0$ (c). Photograph of the ceramic block with a relative permittivity of 34 is shown in the center inset.

This interesting property of the photonic doping verifies again the zeroth-order resonance in the waveguide-emulated ENZ environment.

III. Experimental Verification

To experimentally validate the proposed concept of doped ENZ antenna with an aperture-spacing-irrelevant operating frequency, the prototypes of the doped ENZ antenna with lengths $L = 0.22\lambda_0$ (12 mm), $0.5\lambda_0$ (27 mm), and $0.72\lambda_0$ (39.3 mm) are fabricated via standard planar circuit board technique on a F4BMX substrate with a dielectric constant of 2.2 and a loss tangent of 0.002. Their photographs are shown in Fig. 10(a)–(c), respectively. The macroscopic photonic dopant, made by zirconia microwave ceramic powder with a dielectric constant of 34.0 and a loss tangent of 0.001, is shown in the center inset of Fig. 10. When assembling, the ceramic block is tightly inserted into the substrate with the same-sized zone been previously etched through, and then a piece of copper sheet is soldered above to keep a

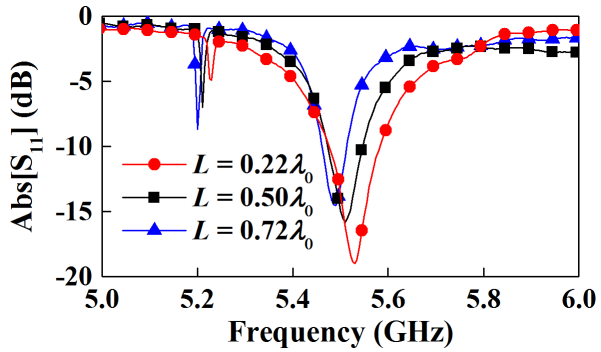

Fig. 11. Measured reflection coefficients of the fabricated doped ENZ antennas with lengths $L = 0.22\lambda_0$, $0.50\lambda_0$, and $0.72\lambda_0$.

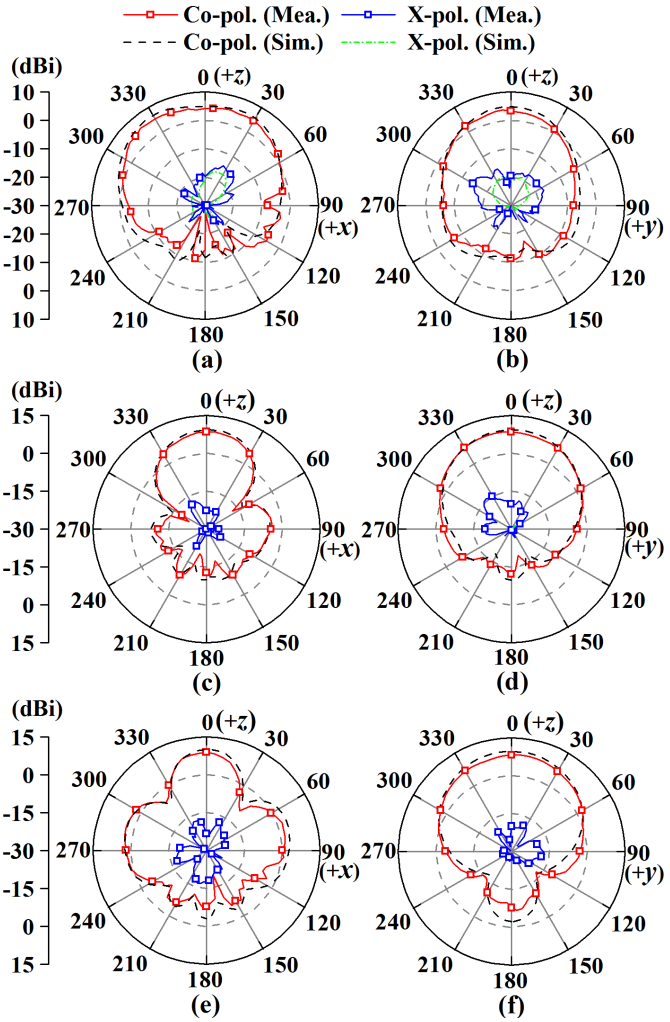

Fig. 12. Measured and simulated realized gain patterns of the designed doped ENZ antennas with length $L = 0.22\lambda_0$ on (a) xz cut plane and (b) yz cut plane. The patterns of the antenna with $L = 0.50\lambda_0$ on (c) xz cut plane and (d) yz cut plane. The patterns of the antenna with $L = 0.72\lambda_0$ on (e) xz cut plane and (f) yz cut plane.

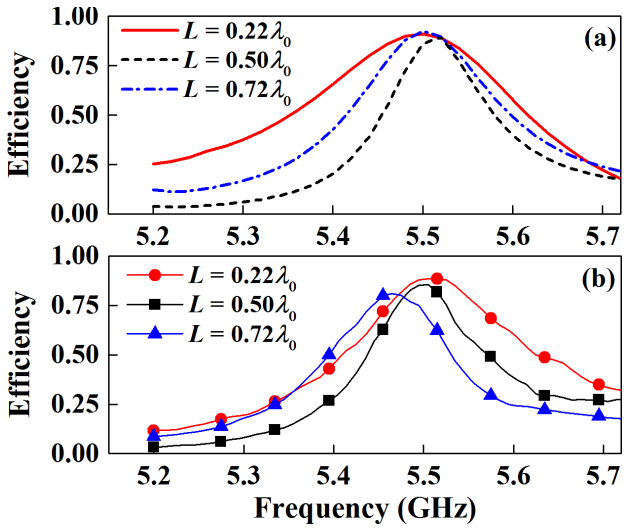

Fig. 13. (a) Simulated and (b) measured total efficiency of the doped ENZ antennas with lengths $L = 0.22\lambda_0$, $0.50\lambda_0$, and $0.72\lambda_0$.

good sealing and conductive effect. Usually, the metamaterial-inspired devices, more or less, may face the deficiency of complex architectures and difficulties in fabrication, as the sophisticated artificial structures have to be used for realizing their peculiar effects. In this aspect, our choice of the planar structure SIW as an ENZ platform benefits the convenient fabrication and integration.

The reflection coefficients of the fabricated doped ENZ antennas are measured with the vector network analyzer Agilent N9917A, and the results are reported in Fig. 11. Although the aperture-to-aperture spacing of the longest prototype [shown in Fig. 10(c)] is larger than three times that of the shortest one [shown in Fig. 10(a)], their operating bands for reflection coefficient better than -10 dB are all round the predesigned frequency $f_0 = 5.5$ GHz, which evidences that the mode of the ENZ resonance is insensitive to the variance in the length of the SIW. The radiation properties of the antennas are evaluated in a standard microwave chamber. The measured realized gains of three prototypes on both xz and yz cut planes at f_0 are shown in Fig. 12, accompanied by the simulation counterparts. The measured realized gains at the broadside for length $L = 0.22\lambda_0$, $0.5\lambda_0$, and $0.72\lambda_0$ are 5.8 dBi, 9.6 dBi, and 8.9 dBi, respectively; the cross-polarization levels are tested better than -20 dB within the HPBW for all the cases. We can also clearly observe from Fig. 12 that the pattern of the antenna on the xz turns to be increasingly directive as the dimension along the x-axis is extended, with the HPBWs for these three prototypes on xz cut plane measured to be 113°, 45°, and 34°, which are largely consistent with the simulation results and the analytical model of doped ENZ antenna. As we manipulate the antenna's dimension only along the x-axis, the beamwidth on the yz plane is nearly unchanged, having an HPBW about 65°. The simulated and measured total efficiencies for the doped ENZ antennas are shown in Fig. 13(a) and (b), respectively, with the measured peak total efficiency near f_0 for all three prototypes higher than 80%. Despite the minor frequency shifts due to fabrication tolerance and experiment imperfect, the measurements are largely in accordance with the results yielded from full-wave simulation. Hence, we have provided a proof of concept for the doped ENZ antenna with an operating frequency irrelevant with its aperture distribution. To fully exploit the dynamic radiation pattern configurability at a fixed frequency, the proposed antenna can furthermore be implemented by the available liquid metal technique along with a stretchable substrate [43].

IV. Conclusion

In this article, by combining the exotic ENZ effect of transverse cutoff mode of the SIW and the concept of macroscopic photonic doping, we propose a kind of SIW antenna with the operating frequency independent on its aperture spacing. In our design, we realize a pair of in-phase effective magnetic currents with a flexibly changeable spacing, which leads to a reconfigurable broadside radiation pattern. It is theoretically studied and numerically demonstrated that, via altering the length of the structure, the directivity of the proposed antenna can be manipulated from around 6 dBi to almost 10 dBi, and what is more, the HPBW allows to be tuned from 110° to near 20°. This conceptually innovative SIW antenna has further been experimentally tested, with a measured designable broadside pattern and length-irrelevant operating band consistent with our theory. Featuring a designable pattern at the same frequency via manipulating the aperture spacing, the proposed doped ENZ antenna can find applications in adaptive wireless communications and spatial energy harvest, and sensing.

References

[1] J. B. Pendry, "Negative refraction makes a perfect lens," *Phys. Rev. Lett.*, vol. 85, no. 18, pp. 3966–3969, Oct. 2000.
[2] N. Engheta and R. W. Ziolkowski, *Electromagnetic Metamaterials: Physics and Engineering Explorations*. Hoboken, NJ, USA: Wiley, 2006.
[3] D. R. Smith, W. J. Padilla, D. C. Vier, S. C. Nemat-Nasser, and S. Schultz, "Composite medium with simultaneously negative permeability and permittivity," *Phys. Rev. Lett.*, vol. 84, no. 18, pp. 4184–4187, May 2000.
[4] V. G. Veselago, "The electrodynamics of substances with simultaneously negative values of ε and μ," *Sov. Phys. Uspekhi*, vol. 10, no. 4, pp. 509–514, 1968.
[5] F. Bilotti, A. Alu, and L. Vegni, "Design of miniaturized metamaterial patch antennas with μ-negative loading," *IEEE Trans. Antennas Propag.*, vol. 56, no. 6, pp. 1640–1647, Jun. 2008.
[6] S. Jahani, J. Rashed-Mohassel, and M. Shahabadi, "Miniaturization of circular patch antennas using MNG metamaterials," *IEEE Antennas Wireless Propag. Lett.*, vol. 9, pp. 1194–1196, 2010.
[7] R. W. Ziolkowski and A. Erentok, "Metamaterial-based efficient electrically small antennas," *IEEE Trans. Antennas Propag.*, vol. 54, no. 7, pp. 2113–2130, Jul. 2006.
[8] S. Lim, C. Caloz, and T. Itoh, "Metamaterial-based electronically controlled transmission-line structure as a novel leaky-wave antenna with tunable radiation angle and beamwidth," *IEEE Trans. Microw. Theory Techn.*, vol. 52, no. 12, pp. 2678–2690, Dec. 2004.
[9] N. Yu *et al.*, "Light propagation with phase discontinuities: Generalized laws of reflection and refraction," *Science*, vol. 334, no. 6054, pp. 333–337, Sep. 2011.
[10] Y. Liu, K. Li, Y. Jia, Y. Hao, S. Gong, and Y. J. Guo, "Wideband RCS reduction of a slot array antenna using polarization conversion metasurfaces," *IEEE Trans. Antennas Propag.*, vol. 64, no. 1, pp. 326–331, Jan. 2016.
[11] T. Liu, X. Cao, J. Gao, Q. Zheng, W. Li, and H. Yang, "RCS reduction of waveguide slot antenna with metamaterial absorber," *IEEE Trans. Antennas Propag.*, vol. 61, no. 3, pp. 1479–1484, Mar. 2013.
[12] E. Saenz, I. Ederra, R. Gonzalo, S. Pivnenko, O. Breinbjerg, and P. de Maagt, "Coupling reduction between dipole antenna elements by using a planar meta-surface," *IEEE Trans. Antennas Propag.*, vol. 57, no. 2, pp. 383–394, Feb. 2009.

[13] X. Wan, L. Zhang, S. L. Jia, J. Y. Yin, and T. J. Cui, "Horn antenna with reconfigurable beam-refraction and polarization based on anisotropic Huygens metasurface," *IEEE Trans. Antennas Propag.*, vol. 65, no. 9, pp. 4427–4434, Sep. 2017.

[14] S. Enoch, G. Tayeb, P. Sabouroux, N. Guérin, and P. Vincent, "A metamaterial for directive emission," *Phys. Rev. Lett.*, vol. 89, no. 21, Nov. 2002, Art. no. 213902.

[15] R. W. Ziolkowski, "Propagation in and scattering from a matched metamaterial having a zero index of refraction," *Phys. Rev. E, Stat. Phys. Plasmas Fluids Relat. Interdiscip. Top.*, vol. 70, no. 4, Oct. 2004, Art. no. 046608.

[16] M. Silveirinha and N. Engheta, "Tunneling of electromagnetic energy through subwavelength channels and bends using ε-near-zero materials," *Phys. Rev. Lett.*, vol. 97, no. 15, Oct. 2006, Art. no. 157403.

[17] Y. Li and N. Engheta, "Supercoupling of surface waves with ε-near-zero metastructures," *Phys. Rev. B, Condens. Matter*, vol. 90, no. 20, Nov. 2014, Art. no. 201107.

[18] G. Lovat, P. Burghignoli, F. Capolino, D. R. Jackson, and D. R. Wilton, "Analysis of directive radiation from a line source in a metamaterial slab with low directivity," *IEEE Trans. Antenna Propag.*, vol. 54, no. 3, pp. 1017–1030, Mar. 2006.

[19] D. Li, Z. Szabo, X. Qing, E.-P. Li, and Z. N. Chen, "A high gain antenna with an optimized metamaterial inspired superstrate," *IEEE Trans. Antennas Propag.*, vol. 60, no. 12, pp. 6018–6023, Dec. 2012.

[20] D. Mitra, A. Sarkhel, O. Kundu, and S. R. B. Chaudhuri, "Design of compact and high directive slot antennas using grounded metamaterial slab," *IEEE Antennas Wireless Propag. Lett.*, vol. 14, pp. 811–814, Dec. 2015.

[21] E. Forati, G. W. Hanson, and D. F. Sievenpiper, "An epsilon-near-zero total-internal-reflection metamaterial antenna," *IEEE Trans. Antennas Propag.*, vol. 63, no. 5, pp. 1909–1916, May 2015.

[22] M. Navarro-Cía, M. Beruete, I. Campillo, and M. Sorolla, "Enhanced lens by ε and μ near-zero metamaterial boosted by extraordinary optical transmission," *Phys. Rev. B, Condens. Matter*, vol. 83, no. 11, Mar. 2011, Art. no. 115112.

[23] S. S. M. Khaleghi, G. Moradi, R. S. Shirazi, and A. Jafargholi, "Microstrip line impedance matching using ENZ metamaterials, design, and application," *IEEE Trans. Antennas Propag.*, vol. 67, no. 4, pp. 2243–2251, Apr. 2019.

[24] J. C. Soric, N. Engheta, S. Maci, and A. Alu, "Omnidirectional metamaterial antennas based on ε-near-zero channel matching," *IEEE Trans. Antennas Propag.*, vol. 61, no. 1, pp. 33–44, Jan. 2013.

[25] J. C. Soric and A. Alu, "Longitudinally independent matching and arbitrary wave patterning using ε-near-zero channels," *IEEE Trans. Microw. Theory Techn.*, vol. 63, no. 11, pp. 3558–3567, Nov. 2015.

[26] Z. Zhou and Y. Li, "Effective epsilon-near-zero (ENZ) antenna based on transverse cutoff mode," *IEEE Trans. Antennas Propag.*, vol. 67, no. 4, pp. 2289–2297, Apr. 2019.

[27] V. Torres *et al.*, "Experimental demonstration of a millimeter-wave metallic ENZ lens based on the energy squeezing principle," *IEEE Trans. Antennas Propag.*, vol. 63, no. 1, pp. 231–239, Jan. 2015.

[28] J. Xiong, X. Lin, Y. Yu, M. Tang, S. Xiao, and B. Wang, "Novel flexible dual-frequency broadside radiating rectangular patch antennas based on complementary planar ENZ or MNZ metamaterials," *IEEE Trans. Antennas Propag.*, vol. 60, no. 8, pp. 3958–3961, Aug. 2012.

[29] V. Pacheco-Peña *et al.*, "Mechanical 144 GHz beam steering with all-metallic epsilon-near-zero lens antenna," *Appl. Phys. Lett.*, vol. 105, no. 24, Dec. 2014, Art. no. 243503.

[30] M. Mitrovic, B. Jokanovic, and N. Vojnovic, "Wideband tuning of the tunneling frequency in a narrowed epsilon-near-zero channel," *IEEE Antennas Wireless Propag. Lett.*, vol. 12, pp. 631–634, 2013.

[31] N. Vojnovic, B. Jokanovic, M. Radovanovic, F. Medina, and F. Mesa, "Modeling of nonresonant longitudinal and inclined slots for resonance tuning in ENZ waveguide structures," *IEEE Trans. Antennas Propag.*, vol. 63, no. 11, pp. 5107–5113, Nov. 2015.

[32] I. Liberal, A. M. Mahmoud, Y. Li, B. Edwards, and N. Engheta, "Photonic doping of epsilon-near-zero media," *Science*, vol. 355, no. 6329, pp. 1058–1062, Mar. 2017.

[33] Z. Zhou, Y. Li, H. Li, W. Sun, I. Liberal, and N. Engheta, "Substrate-integrated photonic doping for near-zero-index devices," *Nat. Commun.*, vol. 10, pp. 1–8, Sep. 2019.

[34] Y. Cassivi, L. Perregrini, P. Arcioni, M. Bressan, K. Wu, and G. Conciauro, "Dispersion characteristics of substrate integrated rectangular waveguide," *IEEE Microw. Wireless Compon. Lett.*, vol. 12, no. 9, pp. 333–335, Sep. 2002.

[35] W. Rotman, "Plasma simulation by artificial dielectrics and parallel-plate media," *IRE Trans. Antennas Propag.*, vol. 10, no. 1, pp. 82–95, Jan. 1962.

[36] C. A. Balanis, *Antenna Theory: Analysis and Design*, 2nd ed. New York, NY, USA: Wiley, 1997.

[37] R. Garg, P. Bhartia, I. Bahl, and A. Ittipiboon, *Microstrip Antenna Design Handbook*. Norwood, MA, USA: Artech House, 2001.

[38] N.-W. Liu, L. Zhu, W.-W. Choi, and X. Zhang, "Wideband shorted patch antenna under radiation of dual-resonant modes," *IEEE Trans. Antennas Propag.*, vol. 65, no. 6, pp. 2789–2796, Jun. 2017.

[39] W. Sun, Y. Li, Z. Zhang, and P.-Y. Chen, "Low-profile and wideband microstrip antenna using quasi-periodic aperture and slot-to-CPW transition," *IEEE Trans. Antennas Propag.*, vol. 67, no. 1, pp. 632–637, Jan. 2019.

[40] D. Huang and Z. Du, "Wideband dual-band dual-polarised antenna with less layer radiating patch," *IET Microw., Antennas Propag.*, vol. 13, no. 8, pp. 1214–1218, Jul. 2019.

[41] F. H. Lin and Z. N. Chen, "Low-profile wideband metasurface antennas using characteristic mode analysis," *IEEE Trans. Antennas Propag.*, vol. 65, no. 4, pp. 1706–1713, Apr. 2017.

[42] Y. Chen, S. Yang, and Z. Nie, "Bandwidth enhancement method for low profile E-shaped microstrip patch antennas," *IEEE Trans. Antennas Propag.*, vol. 58, no. 7, pp. 2442–2447, Jul. 2010.

[43] S. J. Mazlouman, X. Jie Jiang, A. Mahanfar, C. Menon, and R. G. Vaughan, "A reconfigurable patch antenna using liquid metal embedded in a silicone substrate," *IEEE Trans. Antennas Propag.*, vol. 59, no. 12, pp. 4406–4412, Dec. 2011.

Ziheng Zhou received the B.S. degree in physics from Nanjing University, Nanjing, China, in 2017. He is currently pursuing the Ph.D. degree in electrical engineering with Tsinghua University, Beijing, China.

His research interests include metamaterials, metasurfaces, wideband electromagnetic absorbers, electromagnetic sensors, circularly polarized antennas, simultaneous transmitting and receiving antennas, and metamaterial-assisted antennas.

Mr. Zhou received the best student paper awards from the Conference IEEE ISAP 2019. He is serving as a Reviewer for the IEEE TRANSACTIONS ON ANTENNAS AND PROPAGATION and the IEEE ANTENNAS AND WIRELESS PROPAGATION LETTERS.

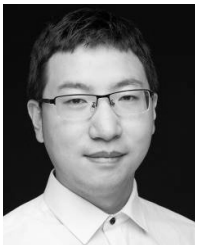

Yue Li (Senior Member, IEEE) received the B.S. degree in telecommunication engineering from Zhejiang University, Zhejiang, China, in 2007, and the Ph.D. degree in electronic engineering from Tsinghua University, Beijing, China, in 2012.

In 2010, he joined the Institute for Infocomm Research (I2R), A∗STAR, Singapore, and the Hawaii Center of Advanced Communication (HCAC), University of Hawaii at Manoa, Honolulu, HI, USA, in 2012, as a Visiting Scholar. In 2012, he joined the Department of Electronic Engineering, Tsinghua University, as a Postdoctoral Fellow. In 2013, he joined the Department of Electrical and Systems Engineering, University of Pennsylvania, Philadelphia, PA, USA, as a Research Scholar. Since 2016, he has been with Tsinghua University, where he is currently an Assistant Professor with the Department of Electronic Engineering. He has authored or co-authored over 130 journal articles and 45 international conference papers, and holds 18 granted Chinese patents. His current research interests include metamaterials, plasmonics, electromagnetics, nanocircuits, mobile and handset antennas, multi-in multi-out (MIMO) and diversity antennas, and millimeter-wave antennas and arrays.

Dr. Li received the Issac Koga Gold Medal from URSI General Assembly in 2017; the Second Prize of Science and Technology Award from the China Institute of Communications in 2017; the Young Scientist Awards from the conferences of PIERS 2019, ACES 2018, AT-RASC 2018, AP-RASC 2016, EMTS 2016, and URSI GASS 2014; the best paper awards from the conferences of ISAP 2019, APCAP 2017, ISAPE 2016, and ICMMT 2016; and the Outstanding Doctoral Dissertation of Beijing Municipality in 2013. He is serving as the Associate Editor for the IEEE TRANSACTIONS ON ANTENNAS AND PROPAGATION, the IEEE ANTENNAS AND WIRELESS PROPAGATION LETTERS, *Microwave and Optical Technology Letters*, and *Computer Applications in Engineering Education*, also as the Editorial Board of Scientific Report.